Article:
Mamalis, D., Floreani, C. and Ó Brádaigh, C.M. (2021) Influence of hygrothermal ageing on the mechanical properties of unidirectional carbon fibre reinforced powder epoxy composites. Composites Part B: Engineering, 225. 109281. ISSN: 1359-8368

https://doi.org/10.1016/j.compositesb.2021.109281

Influence of Hygrothermal Ageing on the Mechanical Properties of Unidirectional Carbon Fibre Reinforced Powder Epoxy Composites

Dimitrios Mamalis[a,b,*], Christophe Floreani[a], Conchúr M. Ó Brádaigh[a]

[a] School of Engineering, Institute for Materials and Processes, The University of Edinburgh, King's Buildings, Edinburgh, EH9 3FB, United Kingdom

[b] Offshore Renewable Energy Catapult, Offshore House, Albert Street, Blyth, NE24 1LZ, UK

*Corresponding author. E-mail address: dimitrios.mamalis@ore.catapult.org.uk

Abstract

A systematic investigation was carried out in this work to evaluate the effect of seawater ageing on the mechanical properties of different composites manufactured with three types of unidirectional carbon fibres, based on a novel powder epoxy system. The flexural behaviour of the samples with and without accelerated seawater ageing was evaluated. A significant strength reduction due to seawater ageing was observed in the composites. Changes within the materials are also evaluated by interlaminar fracture toughness testing and dynamic mechanical thermal analysis. Interlaminar fracture toughness mode-I testing using the Double Cantilever Beam (DCB) test, revealed that the interfacial adhesion differences in combination with the moisture uptake could alter the fracture resistance of the composites, hence emphasising the importance of the interfacial bonding strength. A Finite Element analysis was carried out to gain insight on the important modelling parameters, for mode I dominated failure, and compared with the experimental results. Fracture surface examination by scanning electron microscopy revealed delamination, fibre debonding/bridging and plasticising of resin due to seawater effect.

Keywords:

A. Carbon fibre composites; B. Powder epoxy; C. Hygrothermal Ageing; D. Interface bonding

1. Introduction

Composite structures in the form of layers or laminates are extremely susceptible to crack initiation and propagation along the laminar interfaces in various failure modes. In fact, delamination is one of the most prevalent life-limiting crack growth modes in laminate composites as delamination may cause severe reduction in in-plane strength and stiffness, potentially leading to catastrophic failure of the whole structure [1,2].

Epoxy resins (thermoset polymers) are of significant importance to the engineering field with fibre-reinforced composites based on epoxies being applied widely in the aeronautics, automotive, marine and renewable energy industries [3–9]. Epoxies are characterised by high stiffness, excellent chemical and corrosion resistance, high thermal and mechanical properties, exceptional adhesion to numerous substrates, low shrinkage during curing cycle, outstanding electrical insulating properties, and good processing ability under various conditions [6,10–13]. Hence, the extensive use of epoxy thermosets (as matrices) in a wide range of advanced composite materials is well established. Their inherent fracture toughness limitations lead to brittleness, however, and delamination failures [10,14,15]. In the coating industry, powdered thermosets have been widely adopted, rather than conventional epoxy systems, due to the emission of zero, or near zero, volatile organic compounds (VOC), the absence of solvents, and the potential for extensive utilisation as well as economical and environmentally friendly properties *i.e.* disposability and less hazardous wastes [16,17]. The most significant advantages of the powder epoxies are the characteristically low exothermic reaction during curing process compared to conventional systems and the ability of the powder to melt and flow at elevated temperatures without significantly increasing the degree of cure [17–19]. By utilising the unique properties of the epoxy powders as a composite resin, improvements in the quality and uniformity of the cured material can be achieved [17,20], while also reducing the final production cost. These meaningful processing properties have attracted the interest of tidal and wind energy blade industries where the manufacturing of thick-section composite structures is required e.g. turbine blades or root spars [21].

Composite materials used for marine applications typically consist of carbon or glass fibres embedded in a polymer resin system. Such composites require less maintenance than metals, as they do not oxidise when exposed to seawater. The performance of composite materials under prolonged immersion in water, exposure to wind, rain and sun are generally good when compared to other conventional construction materials (steel, wood etc.). The environmental action including high moisture and high temperature, however, can limit the usefulness of

polymer composites by deteriorating mechanical properties during service. While carbon or glass fibres do not absorb moisture, polymers tend to absorb moisture, which in turn causes swelling and plasticisation effects. More specifically, swelling is related to the development of internal stresses, which is created by the expansion force exerted by the liquid while stretching polymeric chains [22–26]. Plasticisation effects due to moisture uptake can lower the glass transition temperature (T_g) and induce also plastic deformation [22,25,27]. In addition, composites exposed at high temperatures accelerate diffusion rates of moisture and thus accelerate aging mechanism. Moisture uptake in polymer composites mainly affects the properties of the matrix and fibre–matrix interface but also the fibres to some extent, depending on its propensity to absorb water. A reduction in the original properties of composite materials due to environmental effects needs to be well understood and prevented to avoid any unexpected structural failures. It causes two main types of macroscopic effects that decrease the performance of the composite, namely a decrease in the mechanical properties and weight gain of the structure.

The influence of hygrothermal ageing on the mode I fracture toughness has been the subject of numerous studies but there does not seem to be a consensus on the topic. Indeed, some publications have shown that water aging reduces the mode I fracture toughness [28–30] while others show no significant difference [31–33] or even an increase [34–36]. Some studies reported that the Mode I interlaminar fracture toughness of carbon fibre reinforced polymers (CFRPs) increased with increasing moisture content up to a certain amount of moisture followed by a decrease with increase of moisture content up to saturation [26–28]. Hygrothermal ageing in fibre matrix composites has been shown to lead to toughening mechanics such as matrix plasticisation evidenced by a lower Tg found by performing a Dynamic Mechanical and Thermal Analysis (DMTA) [31]. The degradation of the fibre-matrix interface can cause an early formation of fibre-bridging which can increase the initiation toughness [37]. It was shown, however, that exposure to the high temperatures used in accelerated hygrothermal ageing tests creates physical ageing of the resin making it more brittle [38] and hence lowering the fracture toughness. The decrease in matrix strength linked to water absorption can also lead to a decrease in mode I toughness. The opposing effects of these various ageing phenomena on the mode I toughness explain the lack of consistency of published results. In fact, factors such as the water temperature used during hygrothermal ageing and the Tg of the resin or the length of immersion in water can affect the change in mode I toughness observed. It is therefore of interest in this study to understand the influence

of hygrothermal ageing on the mode I interlaminar fracture toughness of carbon fibre powder epoxy composites and to determine if this effect is dependent on the fibre sizing.

The objective of this present investigation is to examine how the matrix and the interfacial bond strength of carbon fibre/epoxy composites are affected by moisture absorption. For this work, three different families of carbon fibres are used to manufacture the composites based on a novel powder epoxy system. The laminates are manufactured using a hand lay-up process followed by an appropriate thermal-curing cycle. A specially designed tensioning apparatus is adopted to apply tension on fibres aiming an enhancement of fibre straightness [39–42]. Composites are evaluated in terms of flexural, interlaminar fracture toughness and viscoelastic performance. Mechanical performance of all laminates is discussed based on interfacial properties before and after immersion. Interfacial adhesion differences are revealed in the flexural and interlaminar properties of the three different families of laminates as well as between the dry and immersed CFRP cases. The difference in mode I delamination behaviour between the hygrothermally aged and dry samples is discussed as well as its effect on crack initiation and propagation mechanisms. A Finite Element Cohesive contact model is developed to give insight on the necessity of using a trilinear cohesive traction-separation rule to model delamination in hygrothermally aged samples to capture the transition in fracture toughness from the onset strain energy release rate (SERR) to the propagation SERR.

2. Experimental procedure

2.1 Materials and composite fabrication

The fabrication of CFRPs was carried out using commercially available continuous tow T700S carbon fibres provided from TORAYCA® (Toray Industries, Inc.) and powder epoxy resin (EC-CEP-0016) supplied from ÉireComposites Teo. (Ireland). Three different carbon fibre types were used to manufacture unidirectional composite materials including T700S - 24K-50C (1% sizing agent), T700S-24K-F0E (0.7% sizing agent) and T700S-24K-60E (0.3% sizing agent) [43]. Note that the sizing agent on the 50C fibres is compatible with epoxy, phenolic, polyester resin systems while the 60E fibre sizing is compatible only with epoxy resin systems according to the supplier [43]. Moreover, the sizing agent on the F0E fibres was mainly compatible with vinyl ester resin systems [43]. Thus, chemical composition differences (distribution of functional groups) as well as different topographical characteristics

(coverage/roughness) between the applied sizing agents are expected to be presented on the surface of the used carbon fibres, as reported by Mamalis et al. acquiring Fourier-transform infrared (FTIR) and Raman spectroscopy results, and Atomic Force Microscopy (AFM) measurements [39,41]. The powder epoxy, with density 1.22 g/cm^3, was used as the matrix to manufacture the composite materials. All initiators-reagents were mixed in the powder, the curing reaction was heat-activated, and the supplier recommended a cure temperature at ~180^{o}C. Moreover, a novel hand lay-up process which used a specially designed tensioning apparatus was adopted such that the carbon fibres were kept in tension during the cure process [39–41]. The thermal cycle applied to all the laminates consisted of a drying stage; an isothermal dwell at 50±1^{o}C for 400 min, B stage (partial curing); isothermal dwell at ~120±1^{o}C for 60 min and a curing cycle with a heating rate of 2±0.2°C/min up to 180±1°C, holding at this temperature at least 90 min, followed by cooling down to room temperature. Laminated composites were prepared by a vacuum bagging technique. Unidirectional carbon fibre powder epoxy composite (CFRP) plates with dimensions of 450 × 250 mm (length × width) and thickness of 3±0.3 mm (16-plies) were fabricated. Furthermore, neat epoxy plates were manufactured following the same thermal cycle as for the composites cases to provide a baseline for comparison. The lay-up of the epoxy plates was fully explained by Mamalis [39–41]. The epoxy powder was distributed evenly on each ply aiming towards a ~60:40 (carbon: epoxy) final volume ratio of the laminate. Fibre volume fraction (FVF) and void content of all the fabricated composites were determined by the acid digestion and ignition (burn-off) methods in accordance with ASTM D3171 (2015). Note that all "dry" specimens were dried in a conventional oven for over 48 hours at ~70°C, prior to testing, aiming to remove any trapped moisture in the samples. Wet specimens were kept in sealed vacuum bags after immersion to avoid moisture evaporation before testing.

2.2 Conditioning

In order to analyse the effect of moisture uptake on the UD composites, laminates containing fibres with the three different sizings as well as the neat epoxy specimens were immersed in a seawater tank. Seawater was obtained directly from the North Sea and changed once a month. The duration of immersion was 3 months, at a constant temperature of 50^{o}C, until ready for testing. The latter was based on previous studies from authors on hygrothermal ageing of this type of powder epoxy composites [44,45]. A minimum of six replicate specimens were immersed. Moisture uptake of the immersed specimens was periodically monitored. Note that

in the initial part of immersion more frequent weight measurements were taken i.e., twice per week, due to the higher rate of moisture uptake in the samples. After this period the weight measurements were taken once per week. All the specimens were wiped to remove any surface moisture, prior to weight measuring. Each specimen was weighed and then returned to the seawater tank. An OHAUS© precision analytical balance with 220 g capacity and a 0.1 mg accuracy was employed. The weight gain of the immersed coupons after exposure to the selected relative humidity environments was measured as a function of time. The moisture content was estimated using the following equation:

$$M = \frac{M_W - M_d}{M_d} \times 100\ (\%)$$

where M is the percentage of gained moisture, M_W is the weight of the wet sample, and M_d is the weight of the dry sample.

Since the width and length of the studied specimens is significantly larger than the thickness, diffusion can be assumed to occur in 1D. The diffusion coefficient, according to Fick's diffusion law can be estimated from the initial linear part of the mass uptake curve with the following equation [46]:

$$D = \frac{\pi}{16M_\infty}\left(\frac{M(t)}{\sqrt{t}}h\right) \quad (3)$$

Where M_∞ is the moisture mass uptake percentage at saturation, t is the immersion time in seconds, h is the specimen thickness and M(t) is the moisture mass uptake as a function of time.

For this reason, the moisture mass uptake is usually plotted against the square root of the immersion time and normalised by the specimen thickness. This allows the diffusion coefficient to be estimated from the slope of the water mass uptake curve. Once the diffusion coefficient is obtained experimentally, the theoretical moisture mass uptake can be predicted using the following equation [46]:

$$M_t = M_\infty\left(1 - \frac{8}{\pi^2}\left[\sum_{n=0}^{\infty}\frac{1}{(2n+1)^2}\exp\left(-\frac{D(2n+1)^2\pi^2 t}{h^2}\right)\right]\right) \quad (4)$$

2.3 Flexural testing

Flexural properties of the UD $[0]_{16}$ CFRPs and the neat epoxy resin plates were determined using a four-point bending configuration according to ASTM D7264 (2007). The tests were carried out by using a universal testing machine Zwick/Roell (model Z010) with a maximum load capacity of 10 kN. The calibration and verification of the measuring system load cell was based on ISO 7500-1:2015 and ASTM E4-2016 standards. The specimens' thicknesses were between 3.3 ± 0.4 mm following a span-to-thickness ratio of 32:1, the standard specimen width was 13 mm and the specimen length was about 20% longer than the support span. The radius of the loading noses and supports was 3 mm. A crosshead speed of 1 mm/min was applied at the compressive face and a linear variable differential transformer transducer (RDP-LVDT) was fitted to measure the absolute linear displacement (position). The flexural properties were determined by loading five or more specimens to failure for each test case; composites and neat epoxy resin, under dry and immersed conditions.

2.4 Interlaminar fracture toughness

The Mode-I (G_{IC}) interlaminar fracture resistance of the UD composites was examined using double cantilever beam test configuration following ASTM D5528-07. The Mode-I tests were carried out at a crosshead displacement of 1 mm/min, at least five specimens for each type of composite were tested. A 13 μm PTFE film was inserted in the in the mid-plane of the laminate; between the 8th and 9th layers, as the initial crack providing a nominal delamination length of $a \approx 63$ mm from the load line. The manufactured laminates were carefully machined to extract the testing specimens with dimension of 150 mm length, 25 mm width and nominal thickness ~3.4 mm. Prior to testing, a white marker was applied at the edges of the specimens and then black dots were painted in order to visualise the crack growth during testing. Tensile loading was applied through two loading blocks adhered to the end of each specimen and video extensometry (UVX - Imetrium systems) was employed to record the crack initiation and propagation for each test. Calculations of the critical energy release rate, G_{IC}, were performed by employing the modified beam theory (MBT) where the rotation at the delamination front was taken in account, as follows:

$$G_{IC} = \frac{3P\delta}{2b(a+|\Delta|)} \quad (1)$$

Where P is the load, δ is the displacement, b is the specimen width, a is the delamination length, and Δ is the horizontal axis intercept from the linear $a - C^{1/3}$ curve. The compliance,C, is the ratio of displacement to corresponding load, δ/P. The value G_{IC} was obtained as the average of G_{IC} values at the ~50mm delamination length.

2.5 Dynamic mechanical thermal analysis (DMTA)

Dynamic mechanical thermal analysis was conducted to characterise the neat epoxy matrix and the UD composites using a Tritec 2000 DMA manufactured by Triton Technology, Ltd. (UK). Samples were placed in the DMTA instrument and oscillated at a frequency of 1 Hz in a single cantilever-bending configuration based on the AITM1-0003 (2010) standard. Tests were run at a slow heating rate of 5°C/min, from room temperature (22°C) to ~190°C and 0.03 mm maximum displacement. The dimensions of all the tested specimens were approx. 35 mm × 10 mm × 3 mm.. The glass transition temperature was determined from the peak of the tan delta curve. Tg values from DMTA tests were obtained from the onset of the change in the slope of the storage modulus (E') curve; Tg_{onset}. More specifically, Tg_{onset} was determined to be the intersection of two slopes from the E' curve, where the first slope was selected at a temperature before the modulus drop step, and the second slope was selected at the temperature indicating the middle point of the modulus drop. In addition, Tg_{loss} and $Tg_{tan\delta}$ values for each case were determined from the peak at loss modulus (E'') curve and the maximum damping (tan δ) ratio i.e., E''/E', respectively.

2.6 Optical characterisation

The surface morphology and the fractured characteristics of the tested/failed composites (dry and immersed flexural specimens) were examined at the nanoscale using a Hitachi S-4700 field emission scanning electron microscope (FE-SEM) with an excitation voltage of 5-20 kV. Prior to examination, CFRP samples were sputter-coated with a thin evaporated layer of gold for a period of 5-8 min reaching a thickness of approximately 100 Å to improve conductivity and prevent charge build-up by the electrons absorbed by the specimen.

3. Results and discussion

3.1 Moisture absorption

In order to investigate the absorption behaviour of the immersed samples exposed to seawater conditions at 50±1°C, the percentage moisture uptake in the composite for the three composites cases and pure epoxy specimens, respectively, is shown in Fig. 1. The moisture mass uptake was plotted against the square root of the immersion time and normalised by the specimen thickness as explained in Section 2.2. The experimental values were plotted against the predicted moisture uptake curve using the 1D Fickian diffusion law described in Eq. 4. It is clear that both the neat powder epoxy resin as well as the three composite materials follow a Fickian behaviour. Moisture absorption rate was high at the beginning of the exposure period of the samples, especially during the first ~30 days in all cases; afterwards, the absorption rate slowly decreased until the end of the study. As can be seen in all curves, the moisture absorption tends towards an equilibrium value, which is material dependent. In the case of neat epoxy specimens, a moisture content of 2.11%, after 91 days of immersion was achieved. In addition, the 50C composites reached a moisture content of 0.9% and the F0E and 60E composites reached values of 0.98% and 0.87%, receptively, after 91 days of immersion. It can be seen from Fig.1 that saturation was not quite reached within the duration of the study but the water mass uptake at saturation was less than 0.1% higher than that obtained in this study for the immersed composites and 0.2% for the neat epoxy resin. According to Fig.1, it would have taken a total immersion time of around 6 months to reach a mass uptake within 0.01% of the saturation value but more than 90% of the mass uptake at saturation was reached in 3 months, justifying the lower immersion time to meet project time constraints. Since carbon fibres are inert and do not absorb moisture, the total moisture content is partitioned into matrix and fibre-matrix interface. It can be noticed that the F0E composites absorbed the highest amount of moisture compared to the other composites, which might be explained by the different chemical composition of the applied sizing agent [39,41,43].

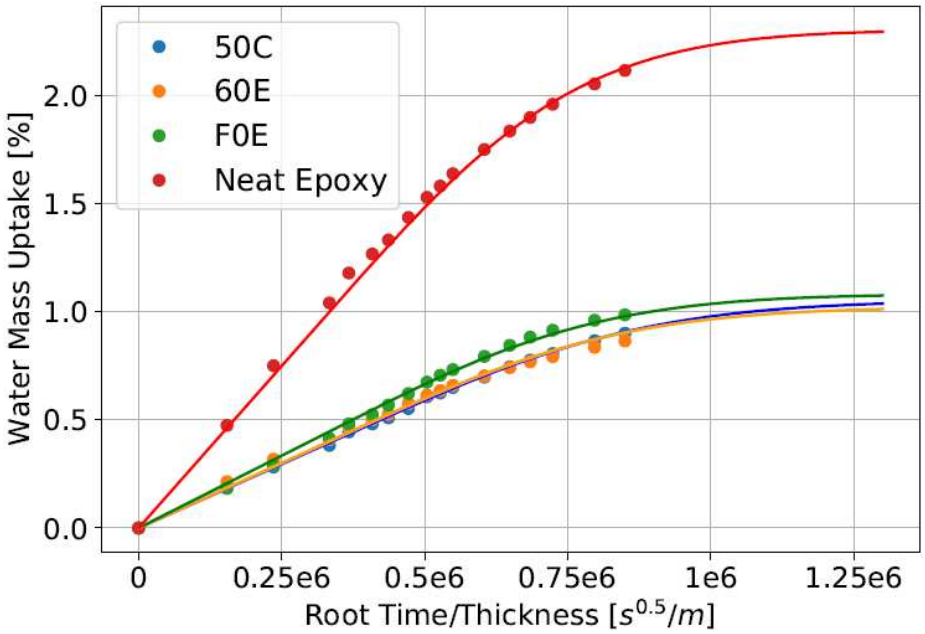

Fig. 1. Experimental moisture mass uptake of the three composite cases i.e., 50C, F0E and 60E, and the pure powder epoxy plate immersed in the seawater and plotted against the theoretical Fickian Diffusion Curves.

3.2 Flexural properties

3.2.1 0° Flexural tests

The results obtained for the longitudinal flexural performance of the conditioned UD CFRPs, after immersion in seawater for ~90 days of exposure at 50°C, in comparison with the dry CFRP cases, all manufactured under tension conditions, are plotted in Fig. 2. The measured flexural strengths for the 50C; ~1180 MPa, and F0E; ~1055 MPa, dry cases were higher than those of the 60E; ~971 MPa, dry composites, as can be seen in Fig 2 (a). The results obtained for the flexural modulus for the same family of specimens are displayed in Fig. 2 (b). For the dry cases, 50C flexural modulus was calculated to be ~117 GPa, while for F0E and 60E cases were 105 GPa and ~99 GPa, respectively. In turn, the 50C composites were characterised by the highest stiffness and strength among the three examined dry composites. Considering that all three types of fibres used have similar mechanical properties [47] and the same fibre volume fraction (FVF) ~59% wt., the differences observed in the flexural properties were attributed to the degree of fibre straightness (as reported from Mamalis et al., where the calculated direction parameter *f* was 0.95, 0.92 and 0.89 for the 50C, F0E and 60E composites, respectively,) and might due to the different sizing agents i.e. amount (and different type) [35–37]. The latter

resulted in different interfacial bonding mechanism between CF fibres/matrix influencing the ultimate flexural performance of the UD composites.

Additionally, Figure 2 (a) shows the results of the flexure strength of the conditioned cases for the three CFRPs. The increase shown in the amount of absorbed seawater for all the conditioned composites cases (Fig. 1) was accompanied by a decrease in the bending resistance. After moisture absorption, the bending strength of the 50C decreased from ~1180 to 930 MPa, the F0E case decreased from ~1055 to ~950 MPa and the 60E case decreased from 971 to 900 MPa, demonstrating a ~23 %, ~11% and ~7% reduction in bending strength, respectively. The 50C composite case was affected to a higher degree from the moisture, showing that the composites with a higher amount of sizing agent on the fibre surface were affected more by the moisture weakening at the interface between fibres/matrix. The decrease in flexure strength was higher for the higher fibre-matrix interfacial strength i.e., 50C composite, but all reduced to a similar level. Moreover, in Fig. 2 (b), flexural modulus values of the three composites cases showed that there are only slight changes in the materials' stiffness. Flexural modulus after immersion of the 50C CFRPs was decreased from ~117 to ~107 while for the F0E and 60E was seen to decrease from ~107 to ~102 GPa and from ~104 to ~98 GPa, respectively. Moisture absorption and thermal ageing led to changes of the structural integrity of polymer composites, in terms of matrix cracking and/or fibre/matrix debonding/discontinuity. The fibre/matrix adhesive damage and a loss of interfacial integrity are dominating mechanisms in polymer composites during environmental ageing.

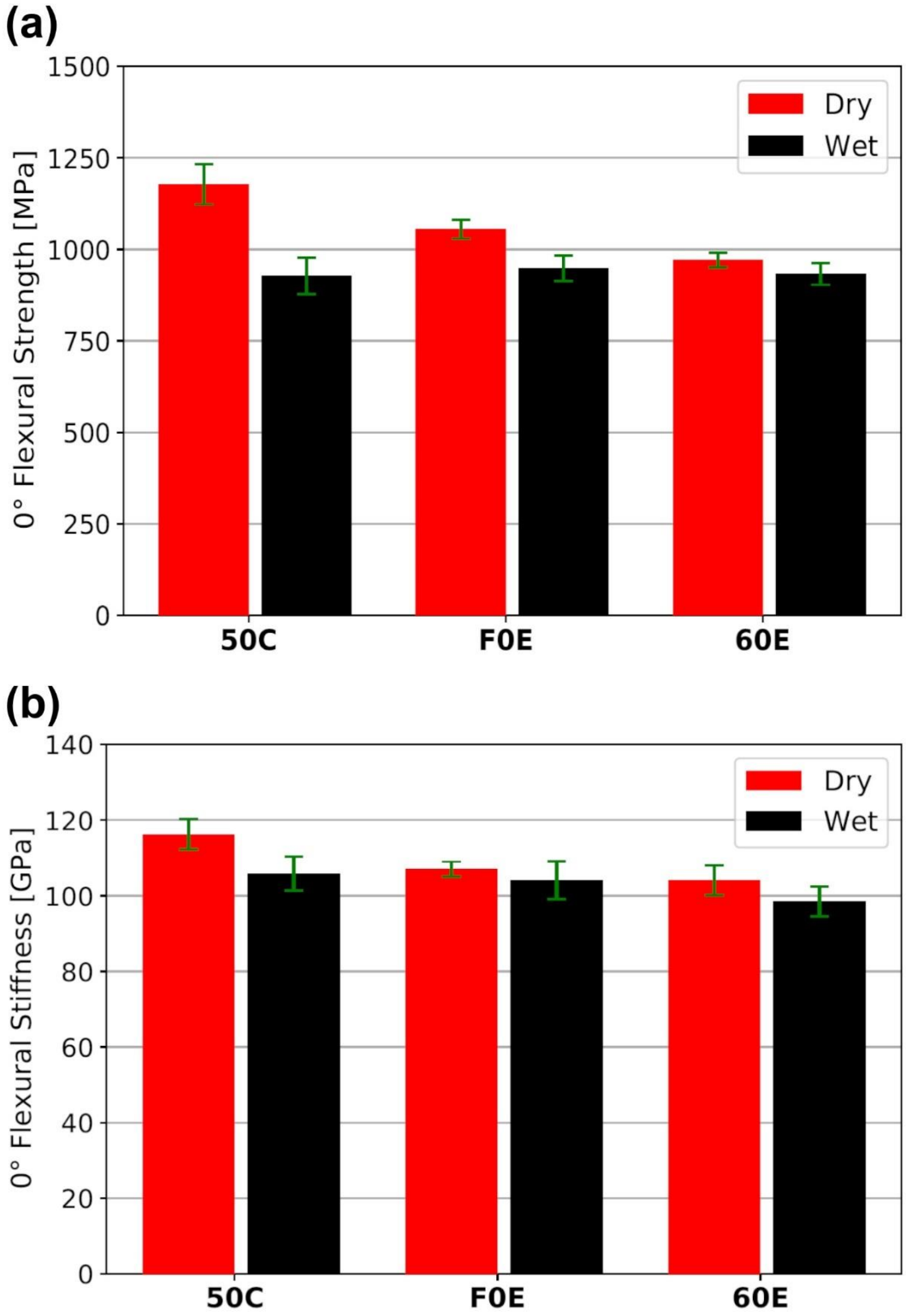

Fig. 2. Overall flexural results (a) strength and (b) modulus of the T700S composite family for the dry and immersed/wet cases. The longitudinal flexural results are average values from ~6 tests for each case i.e., dry and wet. The obtained results were normalised at ~59% FVF for means of comparison.

3.2.2 90^{o} Flexural tests

Transverse flexural results i.e., dry and immersed cases for all composites, under tension conditions, as well as for the pure (powder) epoxy plates are plotted in Fig. 3. The obtained flexural strengths for the dry 50C (~114 MPa) and dry 60E (~105 MPa) cases were remarkably higher; ~34% and ~28%, than those of the dry F0E (~76 MPa) composites, respectively, as displayed in Fig 3 (a). The flexure strength results of the unreinforced epoxy specimens were not plotted as the flexure tests were optimised for testing composites (ASTM D7264) and the epoxy plates were too elastic, hence continuing to bend and reaching the limit of the testing machine. The transverse flexural test of a unidirectional composite can be used as an attractive alternative to the transverse tensile test when determining basic ply properties and a method for evaluating fibre-matrix interfacial bond strength performance. Therefore, in our (dry) cases, 50C and 60E composites exhibited better (stronger) interface bonding and resulted in higher flexural properties. Considering that the same epoxy matrix was used for all composites, the difference observed in the flexural behaviour was connected to the carbon fibre surface properties i.e. sizing agent concentration (and different type) as well as fibre directionality as reported in previous studies [39–41]. One might say that the F0E fibre chemical character i.e., vinyl ester, and the incompatibility with the epoxy matrix affected more the interface bond strength (by decreasing it) and in turn the mechanical performance of the conditioned samples. Overall, the flexural strength (Fig. 3 (a)) of the immersed composites was drastically affected by the moisture uptake by decreasing remarkably the flexural strength of the composites from 50% - 60% in all cases. It is clear that the decrease in strength can be related to amount (and type) of the sizing and the varying fibre straightness (but almost UD) which altered the fibre-fibre interactions and resulted in a different crack initiation and propagation mechanism [39,41,43]. Fig. 3 (b) shows the results obtained for the flexural modulus of the three composites under dry conditions; 50C (~8.3 GPa) > F0E (~7.9 GPa) > 60E (~7.6 GPa). The results of the conditioned panels (composites and neat epoxy) showed a slight decrease following the same trend as seen for the dry cases (50C>F0E>60E). Since the transverse flexural test is matrix dominated, in all the composite cases the flexural moduli were decreased around 2-3%, similarly with the neat epoxy cases, suggesting that the trapped moisture mainly affected the interface between the fibre and the matrix.

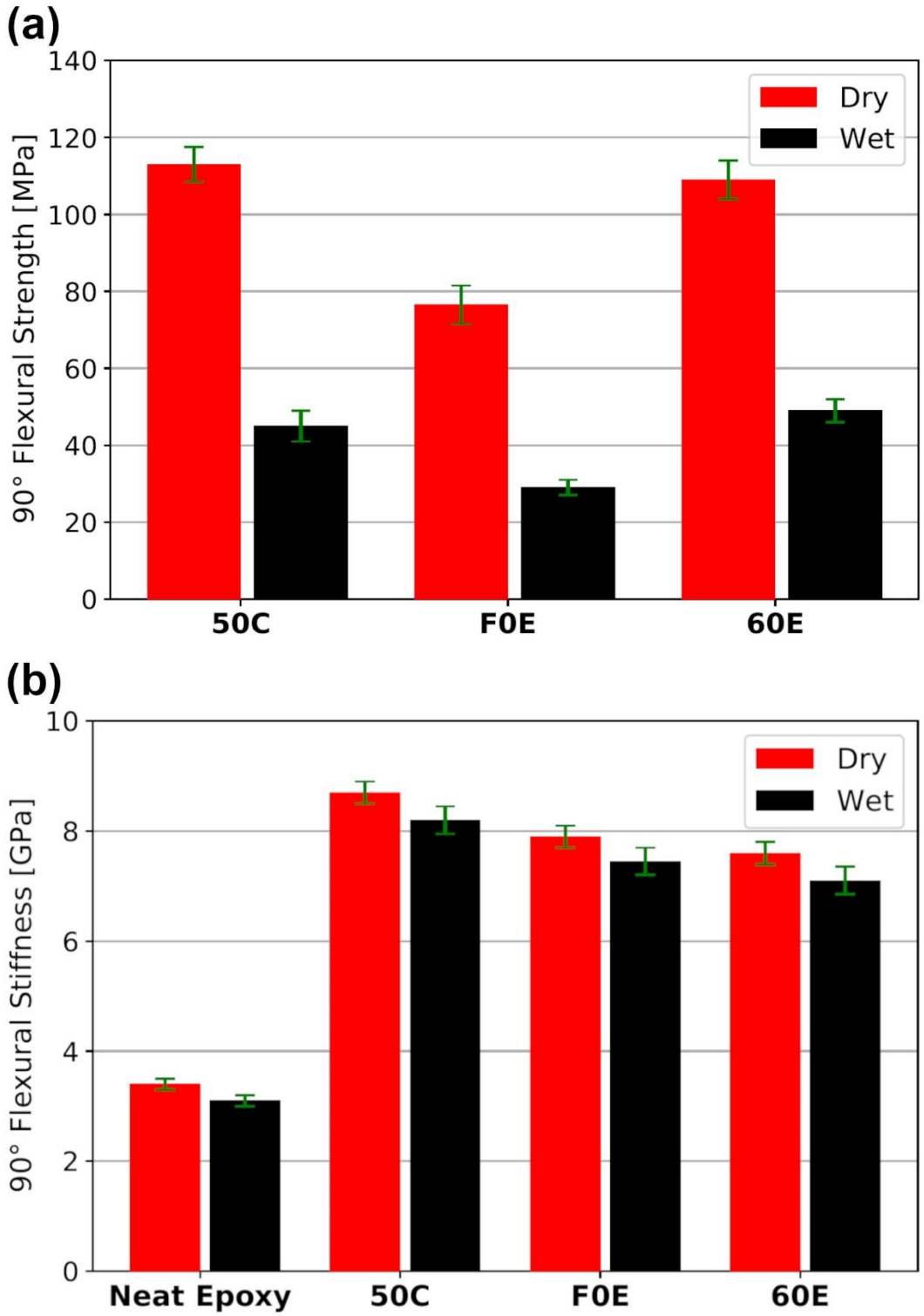

Fig. 3. Transverse flexural (a) strength and (b) stiffness results i.e., dry and conditioned cases, for the T700S family composites as well as for the neat (powder) epoxy blocks. The (90°) flexural values are averages from ~6 tests for each examined case. The obtained results were normalised at ~59% FVF for means of comparison.

3.3 Dynamic mechanical thermal analysis

Characteristic parameters from DMTA testing expressed in terms of a dynamic storage modulus (E'), a dynamic loss modulus (E'') and a mechanical damping term (tan δ). More specifically, the storage modulus characterises the elastic behaviour of the material i.e. stiffness, and the loss modulus characterises the viscous behaviour of the material [48]. In turn, the storage modulus describes the ability of the material to store potential energy per cycle while the loss modulus is related to the energy dissipation in the form of heat upon deformation [49]. The ratio of the loss to the storage modulus (E''/E') is known as the tan δ, which is the dissipation of energy in a material under a cyclic load. As the T_g is a temperature range but not a distinguished thermodynamic transition, in this study, T_g calculations were based on $T_{g,\,onset}$ and $T_{g,\,tan\delta}$ values representing the start and end of this transition regime, respectively.

Moisture has a significant impact on their physical and chemical properties of epoxy matrices as well as on their final performance of composite structures especially in their long-term service life. The absorbed water in a composite usually depresses the glass-transition temperature T_g by plasticising the polymer network and also affects mechanical performance and long-term durability of high performance composites [50–54]. A change in moisture content usually induces swelling that modifies the state of residual stresses in the composite material in addition to the thermal stresses produced during the curing process of the composite material [27,55,56]

The results of dynamic mechanical thermal properties for the 50C, F0E and 60E composites cases as well as the neat (powder) epoxy, under dry conditions and after immersion, are presented in Table 1. Note that the compared composites have similar fibre volume fractions (~59%). $T_{g,\,onset}$ is the first inflection point or the onset of the drop in E' modulus and it is associated with an increase of polymer chain mobility. The $T_{g,\,tan\delta}$ depicts the temperature where the higher amount of polymer chains are in movement - thus it can be related to the interfacial adhesion strength in a composite. Moreover, the incorporation of fibres has an effect on the damping behaviour as additional viscoelastic energy dissipation will occur due to the shear stress concertation at the fibre ends [57]. Considering that the damping parameter in polymer matrices is much higher compared to the composites, the presence of reinforcement is expected to increase elasticity and decrease the viscosity of the composite. It is worth

mentioning that the damping is closely related to the type of fibres, their orientation, fibre volume fraction as well as fibre/matrix interactions, and void content [58,59].

DMTA results of the immersed specimens, in Table 1, show that the glass transition temperature decreases for all cases; neat and composite cases, after the immersion in seawater for a period of ~3-months at 50°C. More specifically, for the neat epoxy case which reached a moisture weight uptake of around (M%) ~ 2.1% (Fig. 2), the $T_{g,\ onset}$ and $T_{g,\ tan\delta}$ temperature values (glass transition regime) were decreased from 105.5 to 71.5 and from 125.6 to 92.2, respectively. Similar behaviour for all the composite cases were observed due to the hygrothermal ageing mechanism, as shown in Table 1. The simultaneous effects of water and temperature cause a synergic result, inducing several phenomena such as plasticisation, molecular degradation, post-curing reactions and formation of pseudo-cross-links by multiple hydrogen bonds with water, giving rise to the formation of a network with different crosslinking densities [60–62]. Furthermore, in the composite the weakening of the fibre/matrix interphase, with de-bonding effects, can occur. The presence of hydrophilic groups in epoxy due to the hydroxyl groups, which can also react with water molecules to form weak hydrogen bonds, is known to cause degradation due to moisture uptake. This indicates that the absorbed water acts as a plasticiser by increasing the mobility of the chains and decreases T_g [31,60,61]. As was expected, neat epoxy revealed a lower glass transition temperature as compared to the composite cases, after immersion.

Table 1 T_g values of the (50C, F0E and 60E) composites and neat epoxy, under dry and wet/immersed conditions. The $T_{g,\ onset}$ and $T_{g,\ tan\delta}$ values are measured at the onset of E'change and maximum of the tan δ curve, respectively. Note that the T_g values obtained are averages from around 6 DMTA tests for each composite and neat epoxy case, respectively.

Material	**Dry conditions**		**Wet conditions**	
	~$T_{g,\ onset}$ (°C)	**~$T_{g,\ tan\delta}$** (°C)	**~$T_{g,\ onset}$** (°C)	**~$T_{g,\ tan\delta}$** (°C)
Neat epoxy	105.5	125.6	71.5	92.2
50C CF/Epoxy	105.8	123.8	77.1	94.2
F0E CF/Epoxy	109.5	125.2	76	92.7
60E CF/Epoxy	104.6	122.1	79.4	95.1

3.4 Microscopic characteristics

Fig. 4 presents high-magnification SEM micrographs of longitudinal distribution of fibres in the UD dry and wet 50C composites, after transverse flexural testing. The observed failure characteristics of the dry CFRP sample revealed a typical brittle matrix fracture (cohesive failure) where failure occurs suddenly. Brittle (unstable) fracture occurs perpendicular to the direction of the applied stress and is characterised by low energy absorption before failure. Fibre fracture, interfacial debonding and characteristic good fibre-matrix adhesion are revealed for the dry 50C CFRP, as shown in Fig. 4 (a). When fibre fracture takes place within a composite, the damage can spread in several ways. Thus, when a strong bonding between the fibre and the matrix is combined with a brittle matrix, the effect of stress concentration at the crack tip can cause the crack to propagate across the whole sample section. Moreover, crack initiation and propagation mechanisms occurred in the interphase region, away from the fibre surfaces, which indicates adequate fibre/matrix adhesion [63,64]. It must be noted that matrix fracture is characterised by multiple fractures locations initiating along the crack front which propagate on slightly different planes. This in turn leads to the development of distinctive fractographic features such as textured microflow, scarps, riverlines and ribbons [63]. More specifically, textured microflow or longitudinal texture, characteristic of brittle fracture, can be clearly observed in Fig. 4 (a) where nodules of the fractured matrix are aligned in the direction of the crack growth, causing this characteristic granular appearance of the fracture surface. Scarps appeared on the fracture surface of the dry CFRPs, attributed to the rapid and sharp steps of the crack propagation. Upon coalescence of crack planes, rather than forming a scarp, distinct ribbons are formed on the surface of the matrix. Another important feature revealed from the fracture surfaces of the CFRPs is the appearance of riverlines (Fig. 4 (a)) resulted from the development of scarps and the convergence of the crack planes [65].

In what follows, the transverse flexural seawater-aged 50C CFRP specimens were examined via scanning electron microscope (SEM). The fractured surfaces of all the tested CFRP specimens after hygrothermal ageing for 3 months at ~50^{o}C appeared to be smoother compared with the dry ones as can be seen in Fig. 4 (b). Characteristically, in wet conditioned cases the matrix tearing was flat and smooth, with the voids contributing to the crack propagation mechanism. The hygrothermally generated porous and weaker interfaces may allow capillary flow of moisture in the composites. As the crack was driven through the interface region within the composite, the hygrothermal degradation of the interface/interphase region directly affected the structural integrity of the composites resulting in a decrease of mechanical properties.

Smoother cracks and bare fibres (constituted a low fracture energy path) with only a few resin fragments attached to the fibres, are apparent on the aged specimen surface compared with the dry CFRP, indicating that immersion leads to an increase in matrix plasticity and a degradation of the fibre-matrix interface. The observed small particles of resin are because of resin degradation produced by hygrothermal ageing and degradation of the fibre/ matrix interface, and they are responsible for the loss of strength capacity of these aged CFRPs. Furthermore, Figure 4 (b) shows evidence of plastic deformation indicating a ductile response (fracture mechanism) of the composite due to the combined effects of plasticising, swelling and hydrolysis. Overall, one can say, that the matrix degradation and the poor matrix/fibre interfacial bonding are essentially responsible for the considerable decrease in mechanical performance at failure of the conditioned composite samples.

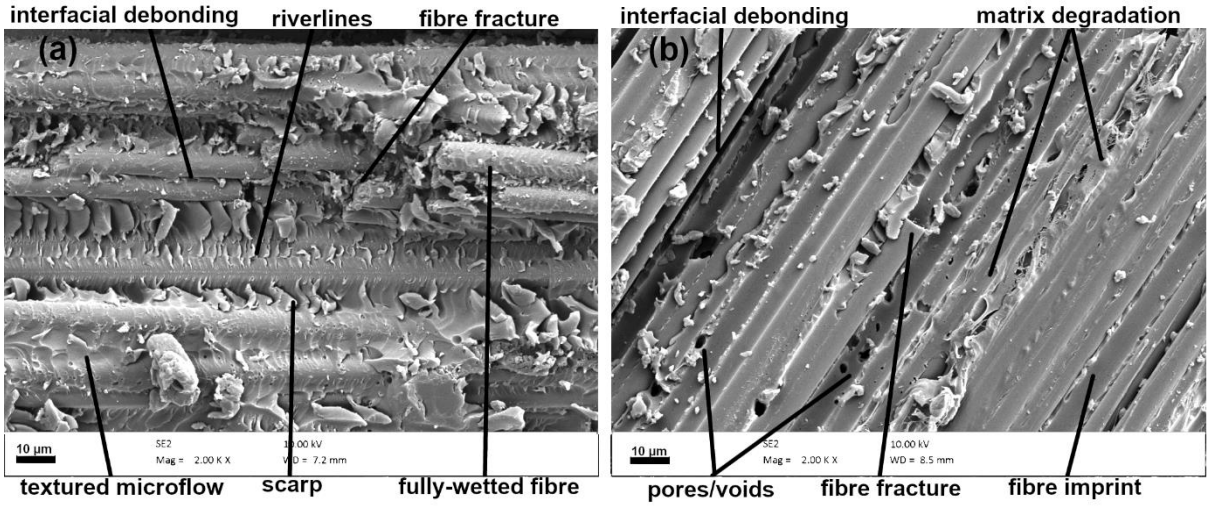

Fig. 4. High magnification (x2000) SEM micrographs of both the (a) dry and (b) wet UD 50C composites. The scale bar represents 10 μm.

3.5 Mode I Interlaminar fracture toughness

The crack length and apparent G_{IC} values were obtained from the high-speed film sequences of each Double-Cantilever Beam (DCB) test, recorded at ~1000 frames per second. The symmetry of both cantilever beams was maintained during the evolution of the test. The results of the mode I DCB tests for all different types of composites both dry and immersed cases are summarised in Figs. 5 and 6. Note that the G_{IC} values refer to averages obtained from the SERR

during crack initiation and propagation according to ASTM D5528 (MBT). The G_{IC} values for the SERR for all composite cases were influenced by the hygrothermal ageing, during the ~3-months conditioning period. Fig. 5 shows the initiation G_{IC} which was selected as the point at which the test samples had a 5% decrease in compliance while Fig. 6 shows the propagation G_{IC} defined in this case as the average of the R-Curve from the 5% compliance point until the end of the test. The initiation G_{IC} values obtained were $G_{IC} \approx 1300$, 900 and 1100 J/m^2 for the 50C, F0E and 60E dry composites cases, respectively. Similarly, the initiation G_{IC} values for the wet composites were $G_{IC} \approx 900$, 550 and 800 J/m^2 for the 50C, F0E and 60E cases, respectively, indicating a decrease in fracture resistance due to hygrothermal ageing. Moreover, the mode I interlaminar fracture toughness values during crack propagation of 50C ($G_{IC} \approx 1535$ J/m^2) and 60E ($G_{IC} \approx 1207$ J/m^2) dry laminates were better than the F0E dry cases ($G_{IC} \approx 1087$ J/m^2), which means the ability of 50C and 60E CFRPs composites containing a crack to resist fracture was better than the F0E ones, as seen in Fig. 6. It is clear from Figs. 5 and 6 that hygrothermal ageing had a far greater influence on the initiation G_{IC} than on the propagation G_{IC} with all three samples showing a significant reduction in the critical SERR (reductions of 34%, 39% and 25% respectively for the 50C, F0E and 60E samples). On the other hand, the effect of hygrothermal ageing on the propagation G_{IC} was less conclusive with a reduction in the critical SERR of 6% and 4% respectively for the 50C and F0E samples but an increase of 21% for the 60E samples.

A likely explanation for this difference in the effect of hygrothermal ageing is that plasticization of the matrix leads to a weakening of the matrix, lower the energy required to propagate a crack. However, as Fig.7 (b) shows, the weakening of the fibre/matrix interface leads to an enhancement of the fibre bridging phenomenon which occurs over a larger region in the wake of the delamination front. This leads to the SERR increasing to a higher value in the hygrothermally aged samples compared to the unaged samples once the delamination front has fully developed and crack propagation becomes stable.

Another phenomenon visible in Fig. 7 (a) is that the region behind the crack opening, over which the fibres are bridging is not very large. The fibres break almost immediately after the crack opening. As the fibre-matrix interface is strong, the sudden fibre breakage has an effect of suddenly lowering the applied load in a DCB test resulting in the stick-slip behaviour. In the case of a hygrothermally aged sample, fibre bridging occurs in a larger leading to a much smoother load-displacement profile as fibres break constantly ahead of the crack tip.

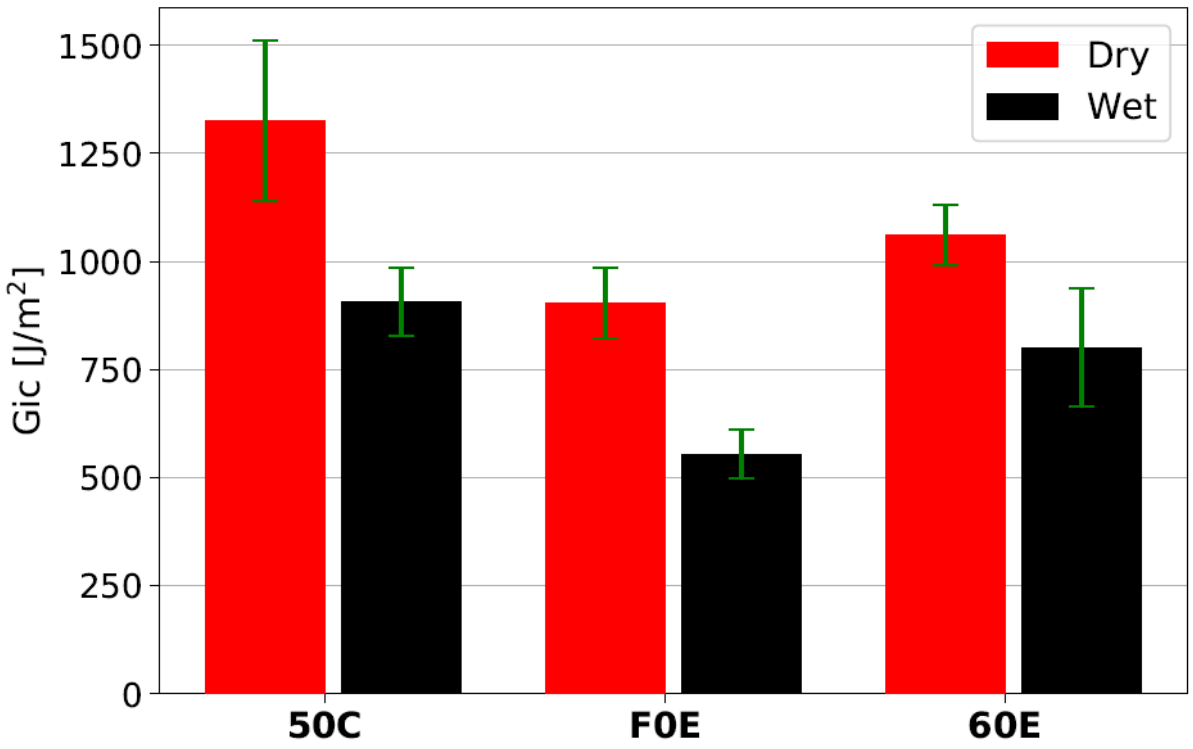

Fig. 5. Initiation G_{IC} for the Mode I DCB tests for all the composites cases. The values are calculated according to ASTM D5528 (MBT) and taken at the 5% compliance point.

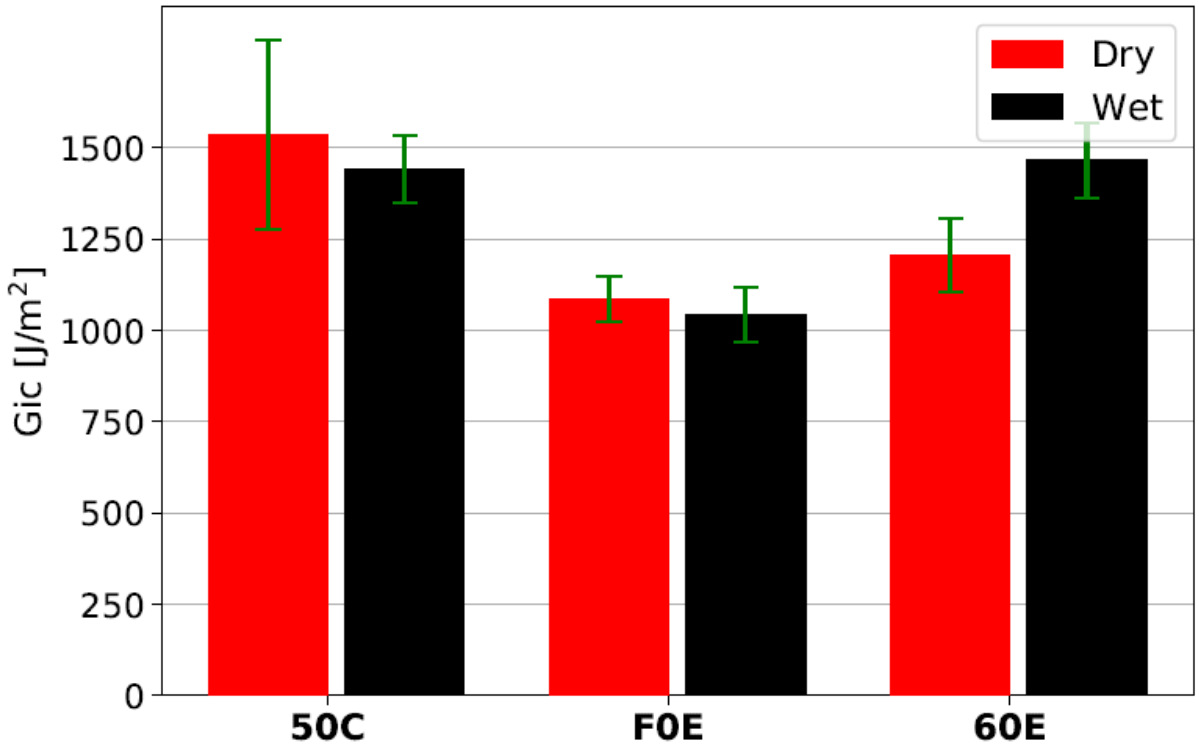

Fig. 6. Propagation G_{IC} for the Mode I DCB tests for all the composites cases. The values are calculated according to ASTM D5528 (MBT) and represent the average R-Curve values from the 5% compliance point until the end of the test.

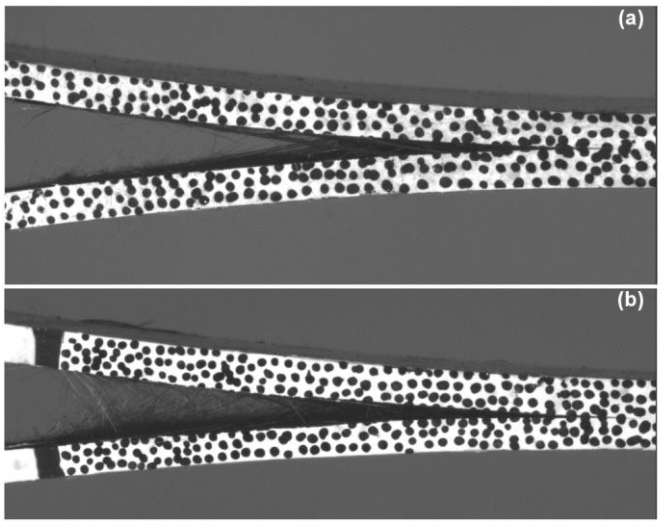

Fig. 7. High speed images of the crack tip zone in detail of 50C (a) dry composite and (b) immersed/wet case. Note that extensive fibre bridging can be observed for the wet CFRP case compared to dry sample.

Fig. 8 shows a comparison of the R-curves obtained for the dry and wet 60E samples which represent the SERR required for crack propagation as the crack advances. It has been shown in

literature that after initial crack extension, toughening mechanisms such as fibre-bridging, fibre pull-out and micro-cracking ahead of the crack front lead to an increase in the SERR up to a steady state value [66,67]. Although the R-curve is not a material property as it also depends on the specimen geometry [68], it was shown that several of its characteristics such as the initiation G_{IC} and the steady-state G_{IC} were constant for a wide range of initial delamination lengths [66]. As the geometry of all the samples tested in this study, however, was the same, differences in the R-curves are linked to changes in the structural response during mode I delamination. Fig. 8 clearly shows that saturated samples had a much slower transition from a low initiation G_{IC} to a stable propagation G_{IC} value. Indeed, a stable propagation value was only reached after 25 mm of crack growth as opposed to 7 mm for the dry samples. Also, the difference between the plateau of the R-curve and the initiation values was far higher for the hygrothermally aged samples compared to the unaged ones where the R-curve is almost perfectly flat. Also, the plateau of the R-curve is at a higher value for the aged samples than that of the unaged ones, which explains the higher propagation G_{IC} measured for the 60E despite a lower initiation G_{IC}. It is worthwhile noting that the same difference in behaviour in the R-curves was observed for the 50C and F0E samples albeit with an increase in the R-curve plateau value for the hygrothermally aged samples that was slightly lower. Since the propagation G_{IC} values are an average of the R-curve, this explains that a reduction in the propagation G_{IC} was measured for the 50C and F0E samples while an increase was measured for the 60E samples.

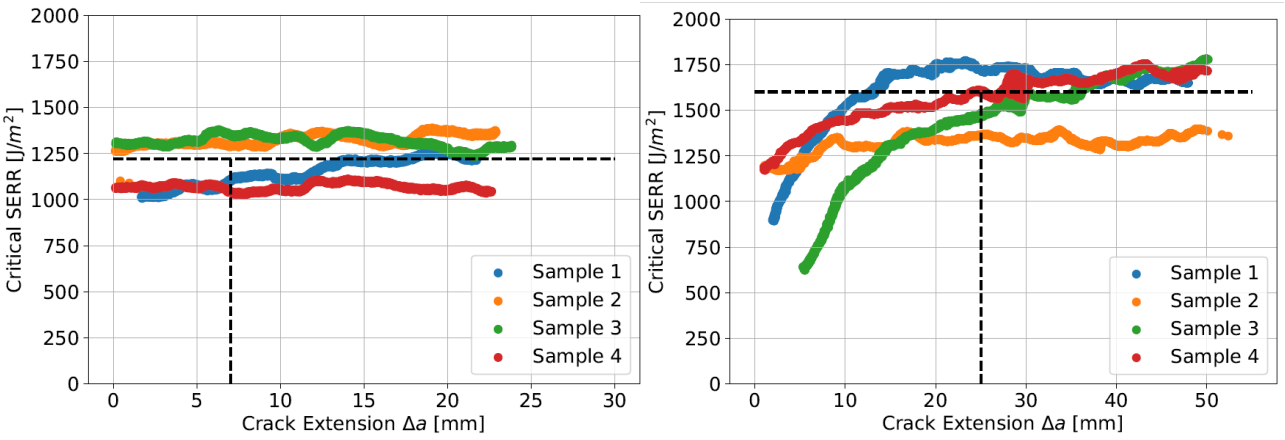

Fig. 8. Typical R-Curves for the 60E DCB dry (left) and wet (right) CFRP samples.

3.6 Finite Element Model of DCB

One of the aims of this study was to conduct a Finite Element simulation of the structural response of the DCB specimens to gain insight into the important modelling parameters to be used in composite delamination studies, for mode I dominated failure. A review paper summarising the modelling strategies used to model DCB samples identified three main numerical methods: VCCT (Virtual Crack Closing Technique), CZM (Cohesive Zone Model) and X-FEM (Extended Finite Element Model) [69]. VCCT models require an initial crack, knowledge of the crack path and these models are already implemented in most commercial FE software. VCCT is applied as a contact criterion between the two DCB arms. CZM models also require knowledge of the crack path but do not need an initial open crack. It can be applied using cohesive elements or through a contact criterion which is more efficient computationally. These cohesive contact elements have a traction separation law. In the case of simple bilinear traction-separation laws, the contact elements are linear-elastic up until their point of maximum stress followed by a linear degradation of the stiffness until it reaches a value of zero, at which point the two elements are no longer considered to be in contact and the crack has propagated. The total area under the traction-separation curve is equal to the critical SERR. This method is already implemented in most commercial FE software and therefore simple to use. Finally, X-FEM allows for an arbitrary crack-propagation using either the VCCT or the CZM formulation and is therefore a better modelling approach when the crack path is unknown. However, the X-FEM method is more computationally expensive and there can be convergence difficulties [69]. As mentioned in the previous section, the SERR is not stable during mode I crack propagation as shown by the R-Curves in Fig. 8. VCCT models and CZM models with bilinear cohesive laws can only account for a single steady value of SERR. Figure 9 shows that either the initiation G_{IC} or the propagation G_{IC} can be used in the model but this either results in an accurate estimation of the peak load at delamination initiation followed by an under-estimation of the stable crack propagation loads or a correct estimation of the stable crack propagation load with an over estimation of the peak load. This inaccuracy was also noticed by other authors [67–69].

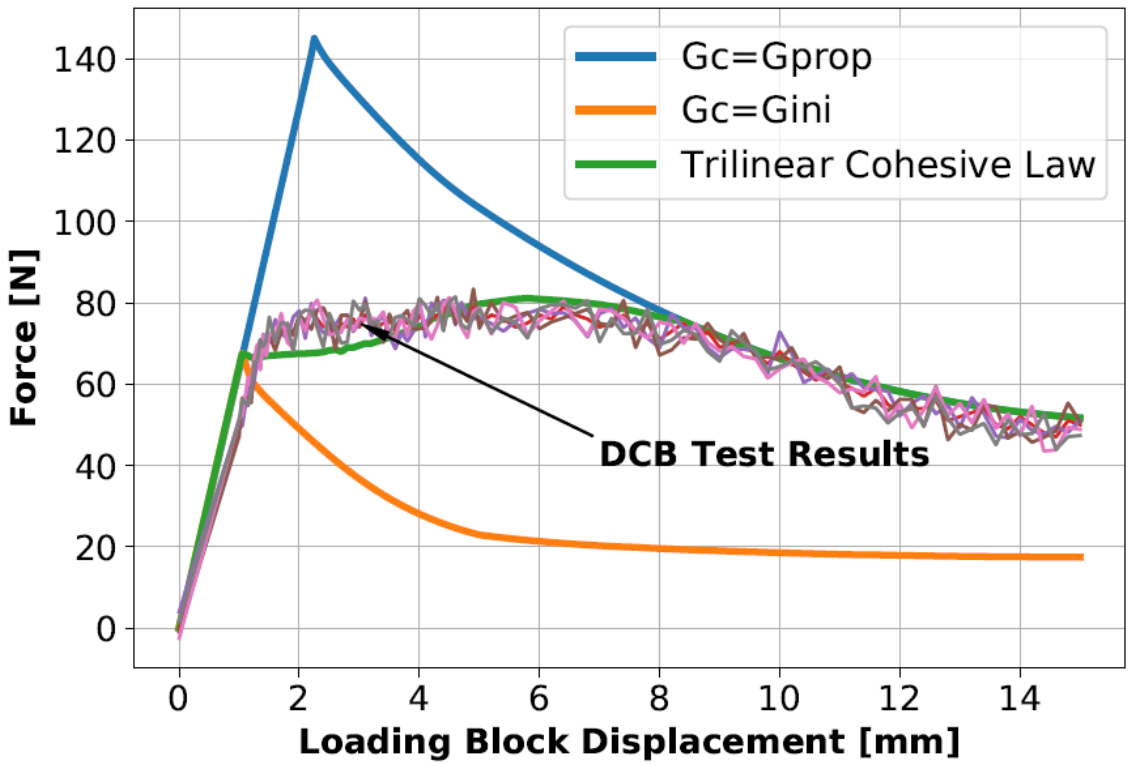

Fig. 9 Force-displacement curves obtained using bilinear and trilinear cohesive laws compared to experimental test result, reproduced from [59]

To improve the overall accuracy of the DCB FE model, more complex cohesive laws have been proposed to account for an increasing G_{IC} value during the delamination propagation. Trapezoidal [70], trilinear [67] and mutli-linear [71] cohesive laws have been proposed to account for fibre bridging and other toughening mechanisms. A multi-linear cohesive law is likely to give the most accurate simulation result but is more complicated to implement as it requires special curve-fitting of the experimental R-curve to obtain the cohesive law. It was decided to use the trilinear cohesive law in this study as it is a compromise between accuracy of the model and complexity. The formulation proposed by Gutkin et al. [67] was used in this simulation. The traction separation law is shown in Fig. 10 and consists of two main triangles. The area under the first triangle corresponds to the initiation G_{IC} while the area under the second one corresponds to the difference between the propagation and initiation G_{IC}.

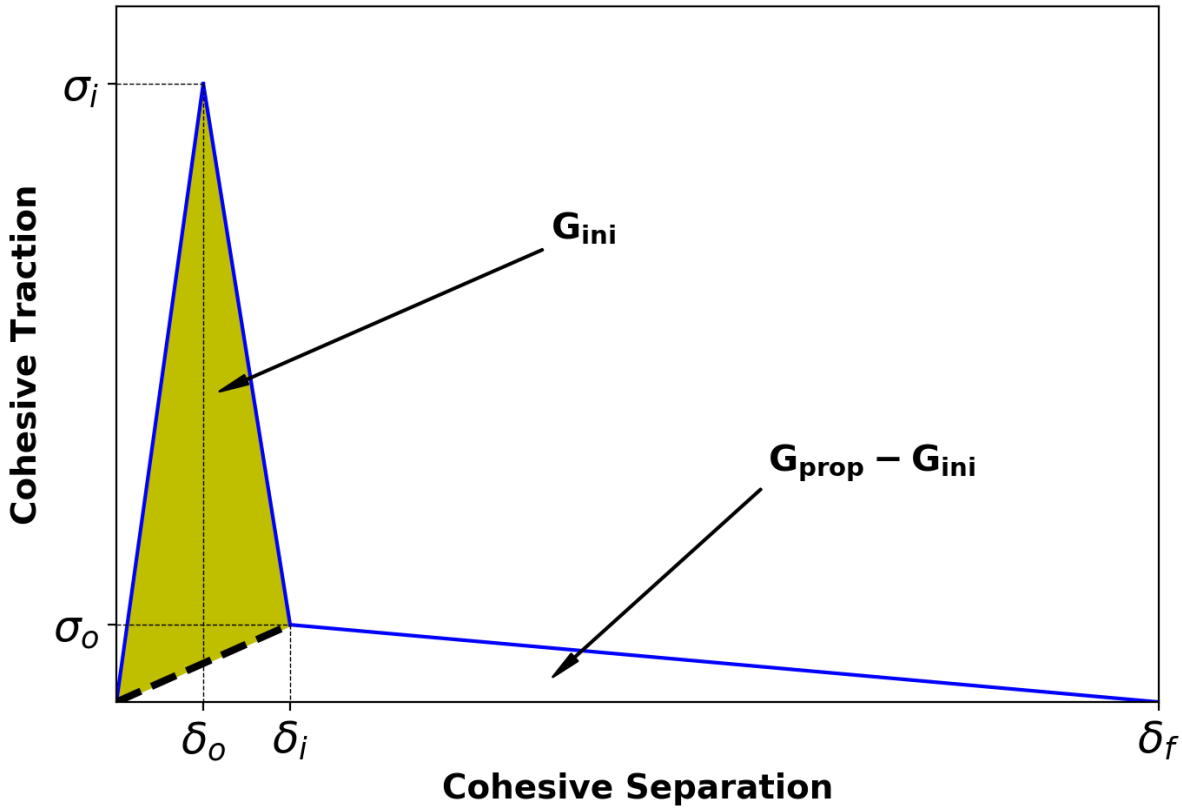

Fig. 10. Cohesive trilinear traction separation law, reproduced from [67].

The cohesive law is defined as:

$$\sigma = \begin{cases} K\delta & for\ \ 0 \le \delta \le \delta_0 \\ \dfrac{\sigma_0}{\delta_i - \delta_0}[(r-1)\delta + (\delta_i - r\delta_0)] & for\ \delta_0 \le \delta \le \delta_i \\ \dfrac{r\sigma_0}{\delta_f - \delta_i}(\delta_f - \delta) & for\ \ \delta_i \le \delta \le \delta_f \end{cases}$$

Where K is the gradient of the linear section of the Cohesive law, r is the ratio between the intermediate strength σ_i and the cohesive strength σ_o, δ_i is the intermediate separation and δ_f is the separation at failure. The cohesive law is derived from the experimental R-curves obtained during DCB tests. Refer to the work of Gutkin et al. [67] for an exact formulation of the traction-separation law.

A 2D plane strain DCB model was developed using the commercial FE package Abaqus. A cohesive contact model was applied through a contact-based criterion between the two DCB arms and an initial crack corresponding to the length of the PTFE insert was included in the model. 1,900 CPE4 plane strain elements were used in the model and the mesh was refined

around the crack tip and in the direction of crack propagation with a distance of 0.25mm between nodes, which was found to be sufficiently small to ensure load convergence. A displacement of 50 mm in the vertical direction was applied on the top loading block while all translational degrees of freedom were fixed on the bottom block.

Fig. 11 below shows the comparison between the FE simulation and the experimental force-displacements curves for the F0E wet and dry samples, respectively. It can be observed that both the experimental and FE results show a flatter peak in the force displacement curve which results from the greater increase in the initiation G_{IC} compared to the dry cases.

An investigation into the appropriate initiation G_{IC} value to use was also carried out as part of this FE simulation. The mode I test standard ASTM D5528-13 offers three possibilities for the initiation G_{IC} value to use: 1) at the point of non-linearity of the force-displacement curve; 2) at the point of maximum load; and 3) at the point where the stiffness increase has reached 5%. It was found that the initiation G_{IC} value obtained at the point of non-linearity in the force-displacement curve gave the best prediction of the peak load in the DCB specimen response, the other 2 proposed values giving a larger value of the peak.

A CZM model using a bilinear cohesive law or a VCCT model is often used to predict mode I delamination. This study showed, however, that when using a tough resin system such as powder epoxy, even in the dry case, it is necessary to use a trilinear cohesive law to accurately predict both the peak load as well as the stable crack propagation loads. This was even more true in the case of wet CFRP samples, where the transition from initiation to stable G_{IC} was even more pronounced.

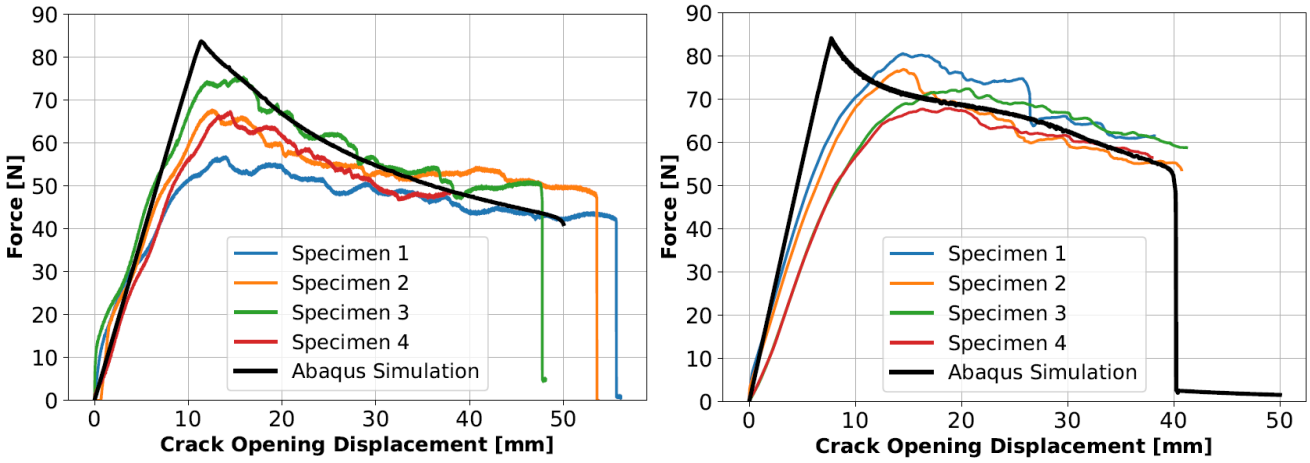

Fig. 11. Comparison between the FE simulation and the experimental force-displacements curves for the F0E wet and dry samples,

4. Conclusions

In this study, unidirectional composites made of three types of reinforcing carbon fibres and a powder epoxy resin, were manufactured through a novel hand lay-up. The three types of carbon fibres differed in the amount of sizing agent, with the 50C, F0E and 60E fibres containing 1%, 0.7% and 0.3% sizing agent, respectively. Interfacial properties were examined and measured through a range of experimental methods including flexural, DCB and DMTA, under dry conditions and after immersion in seawater for 3 months at 50°C.

Fickian moisture absorption kinetics were detected for both the neat epoxy and the composites. A greater moisture uptake at the end of the 3-month immersion time (2.11%) was observed in the neat resin compared to the composites because no moisture is absorbed by carbon fibres. The three composites showed very similar moisture uptake levels at saturation: around 0.9%, with the F0E sample showing a slightly higher uptake of 0.98%. Moisture saturation was not quite reached within the immersion time used in this study. The predicted mass uptake using 1D Fickian diffusion, however, shows that both the neat epoxy and the composites reached a moisture mass uptake greater than 90% of the saturation value.The 0° flexure tests showed that the composite strength in this direction increased as a function of the amount of sizing agent on the fibres, with 50C having the highest strength. In the case of hygrothermally aged samples, however, there was a larger strength reduction of around 20% for the 50C sizing, compared to just 7% for the 60E sizing. It seems that using a greater amount of sizing results in a higher degradation in the fibre-matrix interface strength and in a lower 0° flexural strength of the composites. Additionally, the 90° flexural test was used to evaluate fibre-matrix bond strength

performance. It was shown that, there was a major reduction (more than 50%) in the 90° flexural strength for the hygrothermally aged samples, suggesting a large reduction in the interfacial strength due to the presence of moisture. There was, however, only a minor decrease in the 90° flexural stiffness, which was also matched by a small decrease in the flexural stiffness of the neat epoxy resin.

DMTA analysis of the three composite systems and the neat resin showed a decrease in the Tg by around 35°C for the neat resin compared to a 30°C drop for the three composite systems, which all had Tg peaks around 124°±2°C for the unaged samples, compared to 93°±2°C for the immersed samples. The drop in the Tg highlights the plasticisation effect of moisture uptake on the composites. SEM analysis of the (0° flexural) fracture surfaces for the unaged 50C fibre composites revealed features such as scarps, riverlines and ribbons, which are characteristic of a brittle failure. The broken fibres are still surrounded in resin suggesting a good fibre-matrix interfacial strength. For the hygrothermally aged specimens, a smooth failure surface, characteristic of ductile failure, was observed as well as the presence of bare/clean fibres. This suggests poorer fibre-matrix interfacial strength. The SEM observations showed that there is a transition from a brittle to a ductile failure for the seawater aged samples as well as a clear reduction in the properties of the fibre-matrix interface.

The DCB tests showed that 50C samples had a greater mode I interlaminar fracture toughness than the 60E and F0E samples. Hygrothermal ageing led to a reduction of the initiation G_{IC} of for all three samples but the effect on the propagation G_{IC} was less conclusive with a slight reduction for 50C and F0E samples and an increase for 60E samples. Analysis of the R-Curve showed that in the aged samples, there was a far greater difference between the initiation G_{IC} and the propagation G_{IC}. The R-Curve also reached a plateau at a stable SERR after a much larger crack propagation than for the dry cases. This is linked to the formation of fibre bridging occurring over a greater region ahead of the crack tip. The SERR value at the plateau was slightly higher in the hygrothermally aged samples than that reached in the dry cases for the 50C and F0E samples while it was significantly higher for the 60E samples. This shows that the type (and/or amount) of sizing affects the ageing mechanism on the mode I toughness. There was also a smoother load-displacement curve for the aged samples, as expected, with a reduction in the stick-slip behaviour that was noticed in the dry cases.

Finally, an FE analysis of the DCB samples was carried out to highlight the appropriate modelling strategies to be used in the modelling of delamination in composites containing high toughness resins. It was shown that the large difference between the initiation and propagation

SERR values required the use of a trilinear model and that the value for the initiation SERR should be taken as the point of deviation from linearity in the DCB force-displacement plot.

This work therefore showed that if hygrothermal ageing leads to plasticisation of the matrix and a transition from a brittle to ductile failure, the effect on the mode I fracture toughness can depend on the sizing type and amount. Even though all samples had an increase in fibre bridging, a decrease in the stick-slip behaviour and an increase in the difference between G_{ini} and G_{prop}, the stable propagation G_{IC} value was not affected in the same way by moisture uptake for all the samples. This was explained by the simultaneous presence of toughening mechanisms such as plasticisation of the resin or the enhancement of fibre bridging and embrittling mechanisms such as a reduction in the resin strength and physical ageing of the resin.

Acknowledgments

This work was carried out with funding from MARINCOMP, Novel Composite Materials and Processes for Marine Renewable Energy, Funded under: EU FP7-People, Industry Academia Partnerships and Pathways (IAPP), Project reference: 612531. We also acknowledge funding from POWDERBLADE, Commercialisation of Advanced Composite Material Technology: Carbon-Glass Hybrid in Powder Epoxy for Large Wind Turbine Blades, Funded under: EU Horizon 2020, Fast Track to Innovation Pilot, Project reference: 730747. The authors thank Composites Testing Laboratory (Ireland), for performing a series of tests for this work.

References

[1] Bak BL V., Sarrado C, Turon A, Costa J. Delamination Under Fatigue Loads in Composite Laminates: A Review on the Observed Phenomenology and Computational Methods. Appl Mech Rev 2014;66. doi:10.1115/1.4027647.

[2] Pascoe JA, Alderliesten RC, Benedictus R. Methods for the prediction of fatigue delamination growth in composites and adhesive bonds – A critical review. Eng Fract Mech 2013;112–113:72–96. doi:10.1016/J.ENGFRACMECH.2013.10.003.

[3] Shams SS, El-Hajjar RF. Overlay patch repair of scratch damage in carbon fiber/epoxy laminated composites. Compos Part A Appl Sci Manuf 2013;49:148–56. doi:10.1016/j.compositesa.2013.03.005.

[4] Tehrani M, Boroujeni AY, Hartman TB, Haugh TP, Case SW, Al-Haik MS. Mechanical characterization and impact damage assessment of a woven carbon fiber reinforced carbon nanotube–epoxy composite. Compos Sci Technol 2013;75:42–8. doi:10.1016/j.compscitech.2012.12.005.

[5] Soutis C. Carbon fiber reinforced plastics in aircraft construction. Mater Sci Eng A 2005;412:171–6. doi:10.1016/j.msea.2005.08.064.

[6] Penn L, Wang H. Epoxy resins. In: Peters ST, editor. Handb. Compos. 2nd ed., Boston, MA: Springer US; 1998, p. 48–74. doi:10.1007/978-1-4615-6389-1.

[7] Graham-Jones J, Summerscales J. Marine applications of advanced fibre-reinforced composites. Amsterdam : Elsevier Ltd.; 2016.

[8] Figliolini AM, Carlsson LA. Mechanical properties of carbon fiber/vinylester composites exposed to marine environments. Polym Compos 2014;35:1559–69. doi:10.1002/pc.22809.

[9] Brøndsted P, Lilholt H, Lystrup A. COMPOSITE MATERIALS FOR WIND POWER TURBINE BLADES. Annu Rev Mater Res 2005;35:505–38. doi:10.1146/annurev.matsci.35.100303.110641.

[10] Rafique I, Kausar A, Muhammad B. Epoxy Resin Composite Reinforced with Carbon Fiber and Inorganic Filler: Overview on Preparation and Properties. Polym Plast Technol Eng 2016;55:1653–72. doi:10.1080/03602559.2016.1163597.

[11] Guo H, Huang Y, Liu L, Shi X. Effect of epoxy coatings on carbon fibers during manufacture of carbon fiber reinforced resin matrix composites. Mater Des 2010;31:1186–90. doi:10.1016/j.matdes.2009.09.034.

[12] Paiva JMF de, Mayer S, Rezende MC. Comparison of tensile strength of different carbon fabric reinforced epoxy composites. Mater Res 2006;9:83–90. doi:10.1590/S1516-14392006000100016.

[13] Zhang K, Gu Y, li M, Zhang Z. Effect of rapid curing process on the properties of carbon fiber/epoxy composite fabricated using vacuum assisted resin infusion molding. Mater Des 2014;54:624–31. doi:10.1016/j.matdes.2013.08.065.

[14] Meijer HEH, Govaert LE. Mechanical performance of polymer systems: The relation between structure and properties. Prog Polym Sci 2005;30:915–38. doi:10.1016/j.progpolymsci.2005.06.009.

[15] Kong J, Ning R, Tang Y. Study on modification of epoxy resins with acrylate liquid rubber containing pendant epoxy groups. J Mater Sci 2006;41:1639–41. doi:10.1007/s10853-005-1862-6.

[16] Flanagan T, Maguire J, O Brádaigh C, Mayorga P, Doyle A. Smart Affordable Composite Blades for Tidal Energy. EWTEC11, 2015.

[17] Maguire JM, Nayak K, Ó Brádaigh CM. Characterisation of epoxy powders for processing thick-section composite structures. Mater Des 2018;139:112–21. doi:10.1016/J.MATDES.2017.10.068.

[18] Belder E., Rutten HJ., Perera D. Cure characterization of powder coatings. Prog Org Coatings 2001;42:142–9. doi:10.1016/S0300-9440(01)00149-7.

[19] Robert C, Pecur T, Maguire JM, Lafferty AD, McCarthy ED, Ó Brádaigh CM A novel powder-epoxy towpregging line for wind and tidal turbine blades. Compos Part B Eng 2020;203:108443. doi:10.1016/j.compositesb.2020.108443.

[20] Maguire JM, Simacek P, Advani SG, Ó Brádaigh CM. Novel epoxy powder for manufacturing thick-section composite parts under vacuum-bag-only conditions. Part I: Through-thickness process modelling. Compos Part A Appl Sci Manuf 2020;136:105969. doi:10.1016/j.compositesa.2020.105969.

[21] Ó Brádaigh CM, Doyle A, Doyle D, Feerick PJ. Electrically-heated ceramic composite tooling for out-of-autoclave manufacturing of large composite structures. SAMPE J 2011;47:6–14.

[22] Lin YC, Chen X. Moisture sorption–desorption–resorption characteristics and its effect on the mechanical behavior of the epoxy system. Polymer (Guildf) 2005;46:11994–2003. doi:10.1016/J.POLYMER.2005.10.002.

[23] Núñez L, Villanueva M, Fraga F, Núñez MR. Influence of water absorption on the mechanical properties of a DGEBA (n = 0)/1, 2 DCH epoxy system. J Appl Polym Sci 1999;74:353–8. doi:10.1002/(SICI)1097-4628(19991010)74:2<353::AID-APP17>3.0.CO;2-J.

[24] Toscano A, Pitarresi G, Scafidi M, Filippo M Di, Spadaro G, Alessi S. Water diffusion and swelling stresses in highly crosslinked epoxy matrices. Polym Degrad Stab 2016;133:255–63. doi:10.1016/j.polymdegradstab.2016.09.004.

[25] Nogueira P, Ramírez C, Torres A, Abad MJ, Cano J, Lopez J, et al. Effect of water sorption on the structure and mechanical properties of an epoxy resin system. J Appl

Polym Sci 2001;80:71–80. doi:10.1002/1097-4628(20010404)80:1<71::AID-APP1077>3.0.CO;2-H.

[26] Pitarresi G, Scafidi M, Alessi S, Di Filippo M, Billaud C, Spadaro G. Absorption kinetics and swelling stresses in hydrothermally aged epoxies investigated by photoelastic image analysis. Polym Degrad Stab 2015;111:55–63. doi:10.1016/J.POLYMDEGRADSTAB.2014.10.019.

[27] Alam P, Robert C, Ó Brádaigh CM. Tidal turbine blade composites - A review on the effects of hygrothermal aging on the properties of CFRP. Compos Part B Eng 2018;149:248–59. doi:10.1016/j.compositesb.2018.05.003.

[28] Davies P, Rajapakse YDS, editors. Durability of Composites in a Marine Environment. vol. 208. Dordrecht: Springer Netherlands; 2014. doi:10.1007/978-94-007-7417-9.

[29] LaPlante G, Landry B. The effect of hygrothermal aging on mode I fatigue delamination growth in a carbon/epoxy composites. J Adv Mater 2011;43:79–86.

[30] Lucas JP, Zhou J. The effects of sorbed moisture on resin-matrix composites. JOM 1993;45:37–40. doi:10.1007/BF03222513.

[31] Alessi S, Pitarresi G, Spadaro G. Effect of hydrothermal ageing on the thermal and delamination fracture behaviour of CFRP composites. Compos Part B Eng 2014;67:145–53. doi:10.1016/j.compositesb.2014.06.006.

[32] Tual N, Carrere N, Davies P, Bonnemains T, Lolive E. Characterization of sea water ageing effects on mechanical properties of carbon/epoxy composites for tidal turbine blades. Compos Part A Appl Sci Manuf 2015;78:380–9. doi:10.1016/j.compositesa.2015.08.035.

[33] Khan LA, Mahmood AH, Syed AS, Khan ZM, Day RJ. Effect of hygrothermal conditioning on the fracture toughness of carbon/epoxy composites cured in autoclave/Quickstep. J Reinf Plast Compos 2013;32:1165–76. doi:10.1177/0731684413486367.

[34] Buehler FU, Seferis JC. Effect of reinforcement and solvent content on moisture absorption in epoxy composite materials. Compos Part A Appl Sci Manuf 2000;31:741–8. doi:10.1016/S1359-835X(00)00036-1.

[35] Abanilla MA, Karbhari VM, Li Y. Interlaminar and intralaminar durability characterization of wet layup carbon/epoxy used in external strengthening. Compos Part B Eng 2006;37:650–61. doi:10.1016/j.compositesb.2006.02.023.

[36] de Charentenay F, Harry J, Prel Y, Benzeggagh M. Characterizing the Effect of Delamination Defect by Mode I Delamination Test. Eff. Defects Compos. Mater., ASTM International; 2008, p. 84-84–20. doi:10.1520/stp30199s.

[37] Asp LE. The effects of moisture and temperature on the interlaminar delamination toughness of a carbon/epoxy composite. Compos Sci Technol 1998;58:967–77. doi:10.1016/S0266-3538(97)00222-4.

[38] Le Guen-Geffroy A, Le Gac PY, Habert B, Davies P. Physical ageing of epoxy in a wet environment: Coupling between plasticization and physical ageing. Polym Degrad Stab 2019;168. doi:10.1016/j.polymdegradstab.2019.108947.

[39] Mamalis D, Flanagan T, Ó Brádaigh CM. Effect of fibre straightness and sizing in carbon fibre reinforced powder epoxy composites. Compos Part A Appl Sci Manuf 2018;110:93–105. doi:10.1016/J.COMPOSITESA.2018.04.013.

[40] Mamalis D, Flanagan T, Doyle A, Ó Brádaigh CM. A Carbon Fibre Reinforced Powder Epoxy Manufacturing Process for Tidal Turbine Blades. EWTEC12, 2017.

[41] Mamalis D, Murray JJ, McClements J, Tsikritsis D, Koutsos V, McCarthy ED, et al. Novel carbon-fibre powder-epoxy composites: Interface phenomena and interlaminar fracture behaviour. Compos Part B Eng 2019;174:107012. doi:10.1016/j.compositesb.2019.107012.

[42] Floreani C, Robert C, Alam P, Davies P, Ó Brádaigh CM. Mixed-mode interlaminar fracture toughness of glass and carbon fibre powder epoxy composites—for design of wind and tidal turbine blades. Materials (Basel) 2021;14:2103. doi:10.3390/ma14092103.

[43] Toray Composite Materials America, Inc. 2018. https://www.toraycma.com/page.php?id=661.

[44] Floreani C, Robert C, Alam P, Davies P, Ó Brádaigh CM. Influence of Hygrothermal Ageing on Powder Epoxy Composites for Tidal Turbine Blades. SAMPE J., 2021.

[45] Kennedy CR, Leen SB, Ó Brádaigh CM. Immersed Fatigue Performance of Glass Fibre-Reinforced Composites for Tidal Turbine Blade Applications. J Bio- Tribo-Corrosion 2016 22 2016;2:1–10. doi:10.1007/S40735-016-0038-Z.

[46] Ellyin F, Rohrbacher C. Effect of Aqueous Environment and Temperature on Glass-Fibre Epoxy Resin Composites. J Reinf Plast Compos 2000;19:1405–27. doi:10.1177/073168400772678518.

[47] TORAYCA® T700S DATA SHEET 2018. http://www.toraycfa.com/pdfs/T700SDataSheet.pdf.

[48] Hatakeyama T, Quinn FX. Thermal analysis : fundamentals and applications to polymer science. Wiley; 1999.

[49] Li G, Lee-Sullivan P, Thring RW. Determination of Activation Energy for Glass Transition of an Epoxy Adhesive Using Dynamic Mechanical Analysis. J Therm Anal Calorim 2000;60:377–90. doi:10.1023/A:1010120921582.

[50] Luo S, Leisen J, Wong CP. Study on mobility of water and polymer chain in epoxy and its influence on adhesion. J Appl Polym Sci 2002;85:1–8. doi:10.1002/app.10473.

[51] Lin YC, Chen X. Investigation of moisture diffusion in epoxy system: Experiments and molecular dynamics simulations. Chem Phys Lett 2005;412:322–6. doi:10.1016/J.CPLETT.2005.07.022.

[52] Masoumi S, Valipour H. Effects of moisture exposure on the crosslinked epoxy system: an atomistic study. Model Simul Mater Sci Eng 2016;24:035011. doi:10.1088/0965-0393/24/3/035011.

[53] Pérez-Pacheco E, Cauich-Cupul JI, Valadez-González A, Herrera-Franco PJ. Effect of moisture absorption on the mechanical behavior of carbon fiber/epoxy matrix composites. J Mater Sci 2013;48:1873–82. doi:10.1007/s10853-012-6947-4.

[54] Zafar A, Bertocco F, Schjødt-Thomsen J, Rauhe JC. Investigation of the long term effects of moisture on carbon fibre and epoxy matrix composites. Compos Sci Technol 2012;72:656–66. doi:10.1016/J.COMPSCITECH.2012.01.010.

[55] Fan XJ, Lee SWR, Han Q. Experimental investigations and model study of moisture behaviors in polymeric materials. Microelectron Reliab 2009;49:861–71. doi:10.1016/J.MICROREL.2009.03.006.

[56] Choi H., Ahn K., Nam J-D, Chun H. Hygroscopic aspects of epoxy/carbon fiber composite laminates in aircraft environments. Compos Part A Appl Sci Manuf 2001;32:709–20. doi:10.1016/S1359-835X(00)00145-7.

[57] Akay M. Aspects of dynamic mechanical analysis in polymeric composites. Compos Sci Technol 1993;47:419–23. doi:10.1016/0266-3538(93)90010-E.

[58] Mallarino S, Chailan J-F, Vernet J-L. Interphase study in cyanate/glass fibre composites using thermomechanical analysis and micro-thermal analysis. Compos Sci Technol

2009;69:28–32. doi:10.1016/j.compscitech.2007.10.043.

[59] Clark RL, Craven MD, Kander RG. Nylon 66/poly(vinyl pyrrolidone) reinforced composites: 2. Compos Part A Appl Sci Manuf 1999;30:37–48. doi:10.1016/S1359-835X(98)00083-9.

[60] Alessi S, Conduruta D, Pitarresi G, Dispenza C, Spadaro G. Hydrothermal ageing of radiation cured epoxy resin-polyether sulfone blends as matrices for structural composites. Polym Degrad Stab 2010;95:677–83. doi:10.1016/J.POLYMDEGRADSTAB.2009.11.038.

[61] Alessi S, Conduruta D, Pitarresi G, Dispenza C, Spadaro G. Accelerated ageing due to moisture absorption of thermally cured epoxy resin/polyethersulphone blends. Thermal, mechanical and morphological behaviour. Polym Degrad Stab 2011;96:642–8. doi:10.1016/J.POLYMDEGRADSTAB.2010.12.027.

[62] Zhou J, Lucas JP. Hygrothermal effects of epoxy resin. Part II: variations of glass transition temperature. Polymer (Guildf) 1999;40:5513–22. doi:10.1016/S0032-3861(98)00791-5.

[63] Greenhalgh E. Failure Analysis and Fractography of Polymer Composites . 1st ed. Woodhead Publishing; 2009.

[64] Marston C, Galiotis C. On the failure of unidirectional carbon-epoxy composites Part I: The effect of fibre sizing upon filament fracture and damage evolution. J Mater Sci 1998;33:5311–25. doi:10.1023/A:1004433930232.

[65] Derek H. Fractography observing measuring and interpreting fracture surface topography. Cambridge University Press; 1999.

[66] Shokrieh MM, Heidari-Rarani M, Ayatollahi MR. Delamination R-curve as a material property of unidirectional glass/epoxy composites. Mater Des 2012;34:211–8. doi:10.1016/j.matdes.2011.08.006.

[67] Gutkin R, Laffan ML, Pinho ST, Robinson P, Curtis PT. Modelling the R-curve effect and its specimen-dependence. Int J Solids Struct 2011;48:1767–77. doi:10.1016/j.ijsolstr.2011.02.025.

[68] Suo Z, Bao G, Fan B. Delamination R-curve phenomena due to damage. J Mech Phys Solids 1992;40:1–16. doi:10.1016/0022-5096(92)90198-B.

[69] Heidari-Rarani M, Sayedain M. Finite element modeling strategies for 2D and 3D

delamination propagation in composite DCB specimens using VCCT, CZM and XFEM approaches. Theor Appl Fract Mech 2019;103:102246. doi:10.1016/j.tafmec.2019.102246.

[70] Fernández-Cañadas LM, Iváñez I, Sanchez-Saez S. Influence of the cohesive law shape on the composite adhesively-bonded patch repair behaviour. Compos Part B Eng 2016;91:414–21. doi:10.1016/j.compositesb.2016.01.056.

[71] Jensen SM, Martos MJ, Bak BLV, Lindgaard E. Formulation of a mixed-mode multilinear cohesive zone law in an interface finite element for modelling delamination with R-curve effects. Compos Struct 2019;216:477–86. doi:10.1016/j.compstruct.2019.02.029.